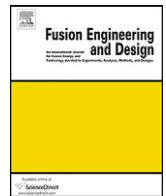




Contents lists available at ScienceDirect

## Fusion Engineering and Design

journal homepage: [www.elsevier.com/locate/fusengdes](http://www.elsevier.com/locate/fusengdes)



# Fusion materials irradiations at MaRIE'S fission fusion facility

Eric J. Pitcher\*

Los Alamos National Laboratory, Los Alamos, NM, USA

### ARTICLE INFO

Article history:  
Available online xxx

Keywords:  
Radiation damage  
Fusion materials  
Primary knock-on atom  
Spallation source

### ABSTRACT

Los Alamos National Laboratory's proposed signature facility, MaRIE, will provide scientists and engineers with new capabilities for modeling, synthesizing, examining, and testing materials of the future that will enhance the USA's energy security and national security. In the area of fusion power, the development of new structural alloys with better tolerance to the harsh radiation environments expected in fusion reactors will lead to improved safety and lower operating costs. The Fission and Fusion Materials Facility (F<sup>3</sup>), one of three pillars of the proposed MaRIE facility, will offer researchers unprecedented access to a neutron radiation environment so that the effects of radiation damage on materials can be measured in situ, during irradiation. The calculated radiation damage conditions within the F<sup>3</sup> match, in many respects, that of a fusion reactor first wall, making it well suited for testing fusion materials. Here we report in particular on two important characteristics of the radiation environment with relevancy to radiation damage: the primary knock-on atom spectrum and the impact of the pulse structure of the proton beam on temporal characteristics of the atomic displacement rate. With respect to both of these, analyses show that F<sup>3</sup> has conditions that are consistent with those of a steady-state fusion reactor first wall.

© 2010 Elsevier B.V. All rights reserved.

## 1. Introduction

The Matter Radiation Interactions in Extremes (MaRIE) concept is a National User Facility to realize the vision of 21st century materials research and development. The Fission and Fusion Materials Facility (F<sup>3</sup>) portion of MaRIE proposes to use the proton linac at Los Alamos National Laboratory (LANL) to drive a spallation neutron source to create an intense irradiation environment for reactor materials testing. Coupled with integrated synthesis and characterization capability, F<sup>3</sup> would also provide the capability for in situ measurements of transient radiation damage, using X-ray and charged particle radiography diagnostics.

The F<sup>3</sup> pillar of MaRIE is predicated on the successful deployment of LANL's proposed Materials Test Station (MTS) [1]. This spallation source facility uses the powerful 1-MW proton beam available at the Los Alamos Neutron Science Center to produce  $10^{17}$  neutrons/s. The MTS is sponsored by the US Department of Energy's Office of Nuclear Energy, with the mission of testing fission reactor fuels and structural materials in a fast neutron spectrum. The current schedule calls for the MTS to begin operation in 2016. An assessment of the MTS irradiation environment [2] shows that, with respect to displacement rate, helium production, and produc-

tion of impurities via transmutation, the MTS has characteristics that match well those expected in the first wall of a fusion reactor.

As part of MaRIE, LANL proposes to augment the MTS with unprecedented in situ diagnostic capability and an increase in beam power over the MTS level of 1 MW. With these augmentations, the MTS becomes the F<sup>3</sup>. The amount of beam power that will drive F<sup>3</sup> is under study, but the goal is to provide researchers with a peak displacement rate of 50 dpa/fpy (full power year), equivalent to an instantaneous rate of  $1.58 \times 10^{-6}$  dpa/s.

## 2. Displacements and gas production

The peak displacement rate in the irradiation regions of F<sup>3</sup> is roughly proportional to (beam power)<sup>0.8</sup>. Assuming a beam power of 1.8 MW driving the F<sup>3</sup>, the range of displacement and He production rates in iron accessible in the irradiation regions is shown in Fig. 1. Each pixel plotted represents a 40-mm<sup>3</sup> volume element in either the fuel (green pixels) or material (orange pixels) irradiation regions. The F<sup>3</sup> offers a broad range of He-to-dpa ratios, from 5 to 33 appm/dpa. This allows scientists to measure materials properties as a function of this important parameter. (For interpretation of the references to color in this paragraph, the reader is referred to the web version of the article.)

As with the peak displacement rate, the irradiation volume is also sensitive to beam power. Fig. 2 shows the minimum displacement rate in iron as a function of irradiation volume. Only those volume elements whose He/dpa ratio is "fusion relevant," that is,

\* Corresponding author at: Los Alamos National Laboratory, P.O. Box 1663, MS H816, Los Alamos, NM 87545, USA. Tel.: +1 505 665 0651.  
E-mail address: [pitcher@lanl.gov](mailto:pitcher@lanl.gov)

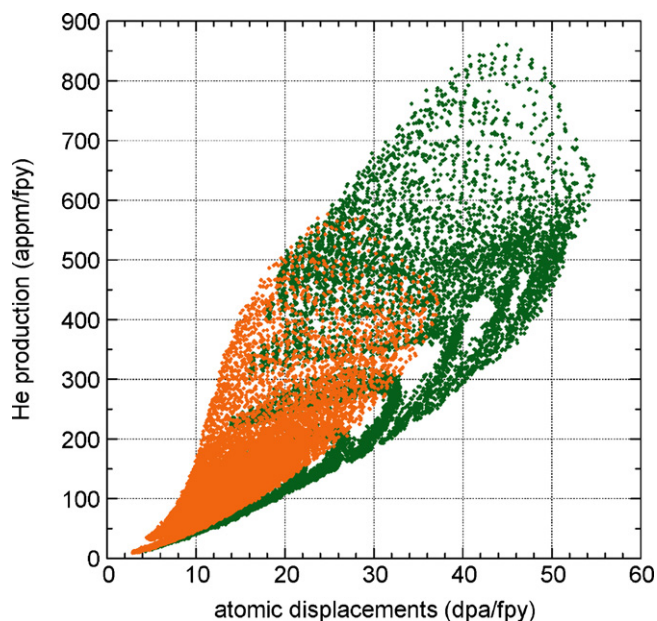


Fig. 1. Displacement and helium production rates for F<sup>3</sup> at beam power of 1.8 MW.

between 8 and 13 appm/dpa, are included in the volume estimate. One can see that, for example, at a beam power of 1.8 MW the displacement rate within a half-liter volume ranges from 12 to 54 dpa/fpy.

### 3. PKA spectra and damage production function

Damage morphology is sensitive to the energy of the recoiling nuclei, or primary knock-on atoms (PKA), inducing lattice displacements. The PKA spectrum depends on the energy spectrum of the neutrons causing the radiation damage. The neutron spectrum at the peak flux position of F<sup>3</sup> is plotted in Fig. 3. Also plotted is the neutron spectrum for the Helium Cooled Lithium Lead (HCLL) blanket of the proposed DEMO fusion reactor. Note that the spectra are

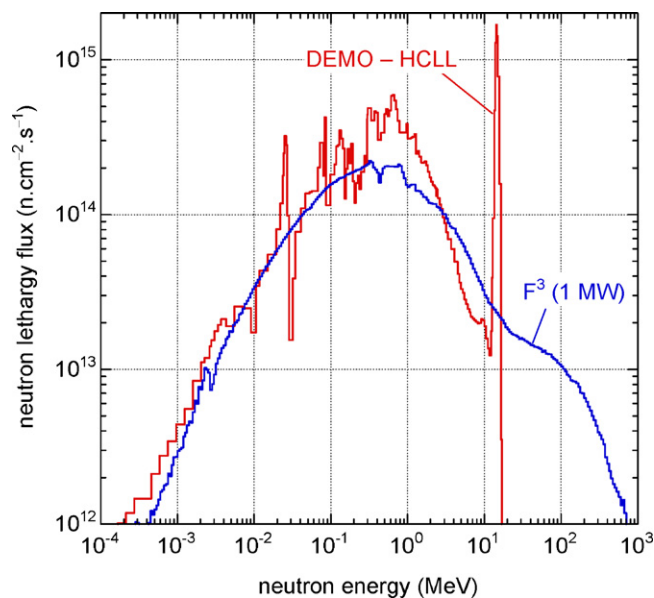


Fig. 3. Neutron flux lethargy spectra for F<sup>3</sup> and the DEMO HCLL.

quite similar below a few hundred keV, while they differ appreciably above 10 MeV. The prominent 14-MeV peak is clearly evident in the DEMO spectrum, as is the high-energy tail of the F<sup>3</sup> spectrum, which extends up to the incident proton beam energy of 800 MeV.

Following the method used by Simakov et al. [3], nuclear recoil spectra for neutron-induced reactions in iron were calculated using the NJOY [4] nuclear data processing code. For neutron energies up to 58.4 MeV, recoil spectra were folded with the neutron spectra plotted in Fig. 3. For the F<sup>3</sup>, nuclear recoils produced by neutrons with energies greater than 58.4 MeV and by protons of all energies were calculated using the radiation transport code MCNPX [5] and its associated post-processing code HTAPE3X. The HTAPE3X and NJOY results were summed to obtain the recoil spectrum for all neutrons and protons. The nuclear recoil, or PKA, spectra calculated in this manner are plotted in Fig. 4. The PKA spectra for the two facilities are in good agreement up to about 50 keV. The highest PKA energy for the DEMO HCLL is 2.7 MeV, whereas for F<sup>3</sup> the PKA

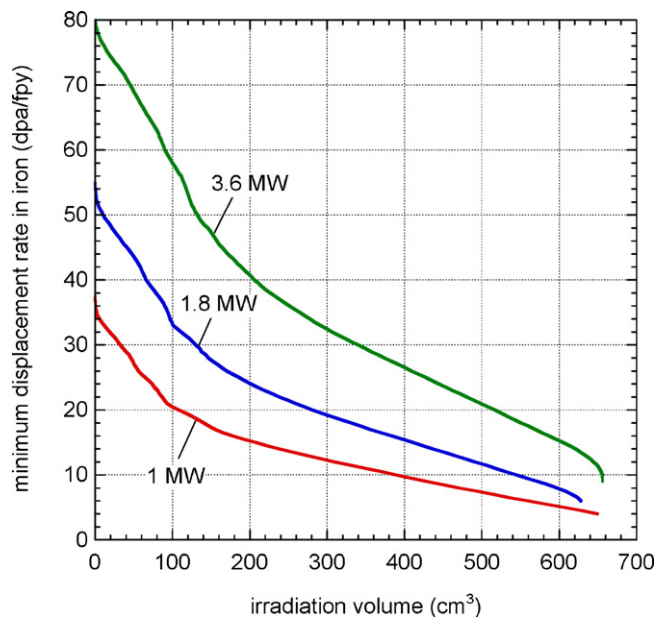


Fig. 2. Displacement rate in iron as a function of volume for three different beam powers. The tallied volume includes only that for which the He/dpa ratio ranges from 8 to 13 appm/dpa.

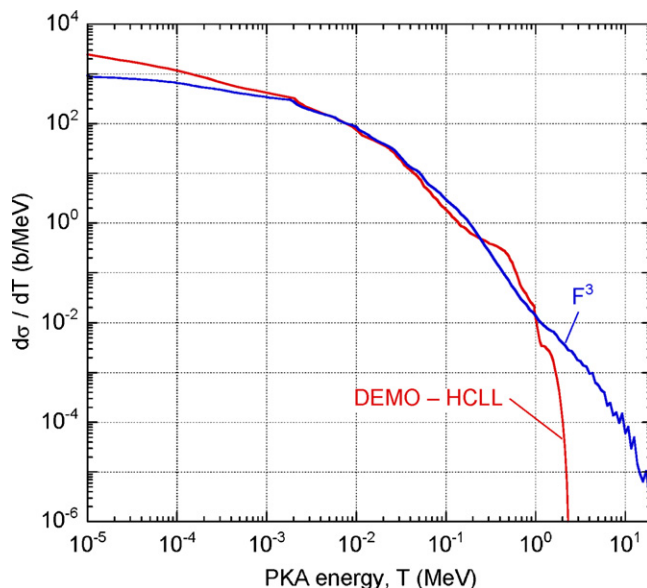


Fig. 4. PKA spectra for the DEMO HCLL and the F<sup>3</sup>.

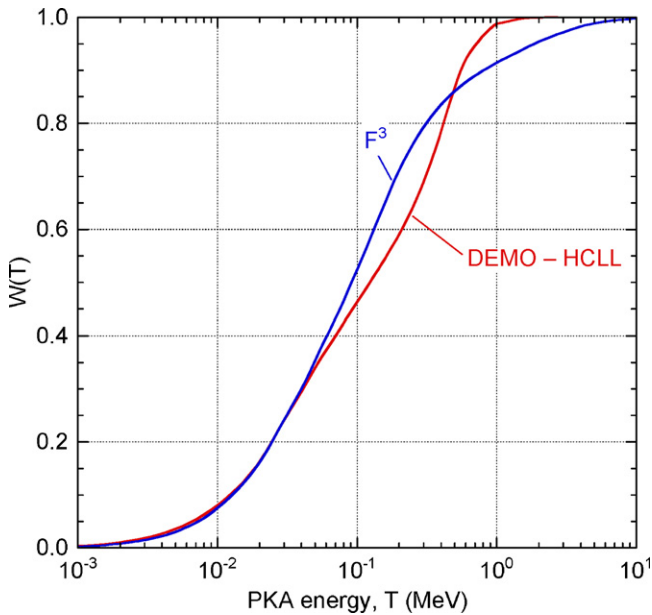


Fig. 5. Damage production functions for DEMO and F<sup>3</sup>.

spectrum extends to 20 MeV. The energetic PKA's are recoils from nonelastic reactions in iron caused by neutrons in the high-energy tail shown in Fig. 3.

One indicator of the influence of neutron spectrum on damage morphology is the damage production function  $W$ , defined as the fraction of total lattice displacements caused by PKA's with kinetic energy less than  $T$ . The  $W(T)$  function is calculated as described by Fischer et al. [6], using the NRT model [7] to calculate the fraction of PKA energy inducing displacements. The damage production functions calculated in this manner for DEMO and the F<sup>3</sup> are shown in Fig. 5. As expected by comparison of the two PKA spectra, good agreement of the damage production functions is seen for the two facilities for  $T < 50$  keV. For DEMO, nearly all displacements are caused by PKA with energies less than 1 MeV. For the F<sup>3</sup>, however, PKA's with  $T > 1$  MeV (0.4% of all PKA's) are responsible for nearly 10% of all displacements. The onset of sub-cascade formation occurs at 10 keV [8], and it may be that damage morphology is not sensitive to differences in the  $W(T)$  function above about 100 keV. If true, then the F<sup>3</sup> will exhibit damage morphology in iron similar to that expected in the DEMO first wall.

#### 4. Displacement rate temporal dependence

The displacement rate in an iron sample placed in the irradiation region of F<sup>3</sup> varies in both space and time. Spatially, the peak displacement rate occurs at beam mid-plane and within the fuel irradiation region between the two spallation target sections, about 5 cm downstream of the spallation target front face (see Refs. [1,2] for descriptions of the geometry).

The pulsed nature of the LANSCE proton beam will influence the time dependence of the displacement rate. The beam structure, shown in Fig. 6, includes both macro- and micro-structure. The beam macropulse is 750  $\mu$ s long, with a repetition rate of 120 pulses per second. The MTS will receive five out of six macropulses produced by the LANSCE accelerator, or 100 pulses per second, which yields a 7.5% beam duty factor. Within each beam macropulse the beam has microstructure, with micropulse width and spacing of 100 ps and 5 ns, respectively, as shown in Fig. 6.

Another factor influencing the temporal dependence of the damage rate is the proposed scheme of rastering the proton beam

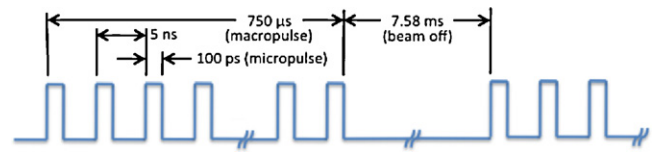


Fig. 6. LANSCE beam pulse structure for F<sup>3</sup>.

on the target. Alternating beam macropulses are directed onto one of the target sections.

For each macropulse, the beam is rastered on the target as depicted in Fig. 7. A slow vertical slew (relative to the horizontal slew) is applied to the beam that passes the beam exactly once over the beam footprint's 60-mm height during the 750- $\mu$ s macropulse, corresponding to a vertical slew rate of 80 m/s. In the horizontal direction, the proposed beam raster system uses a combination of 20- and 60-kHz magnets to provide nearly linear oscillation of the beam that traces the beam back and forth over the 15-mm beam footprint width every 50  $\mu$ s, for a horizontal slew rate of 600 m/s. This cycle (back and forth) is repeated 15 times over the 750- $\mu$ s macropulse. When combined with the vertical slew, the raster scheme produces the raster pattern depicted in Fig. 7. The beam optics have been designed to produce a nominal beam spot size on target of 3 mm FWHM horizontal by 8 mm FWHM vertical, with nominally Gaussian distribution in both dimensions.

The radiation transport code MCNPX was used to calculate the time dependence of atomic displacements in iron at the position in the fuel irradiation region where the time-averaged radiation damage rate is highest. The raster pattern was approximated in the MCNPX simulation by stepping the beam over the raster pattern in 5- $\mu$ s increments. That is, the beam was allowed to dwell in a spot for 5  $\mu$ s, then moved to the next point for 5  $\mu$ s. A mesh tally of the source protons confirmed the suitability of this approximation. In reality, the 750- $\mu$ s macropulse is comprised of 150,000 micropulses. As this was too much detail to include in the simulation, the impact of micropulse structure on the peak displacement rate was assessed by simulating a train of 20 micropulses. These were placed at exactly 375–375.1  $\mu$ s within the beam macropulse, where the beam passes the mid-plane and closest to the tallied radi-

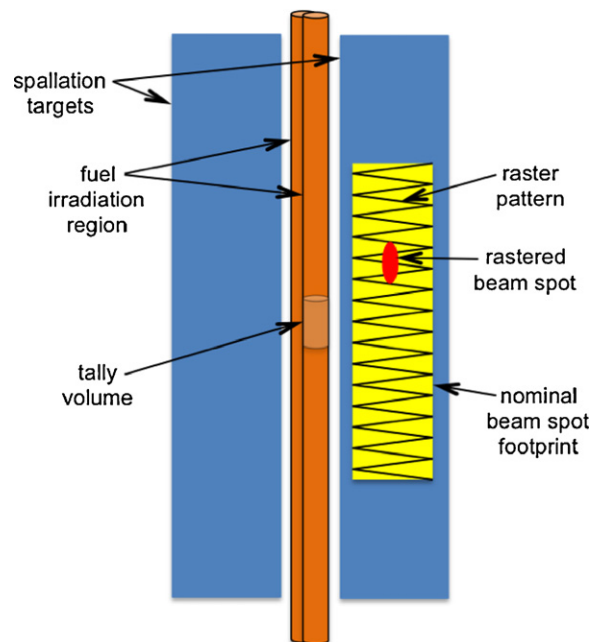


Fig. 7. Geometric representation of the beam raster pattern on the F<sup>3</sup> target.

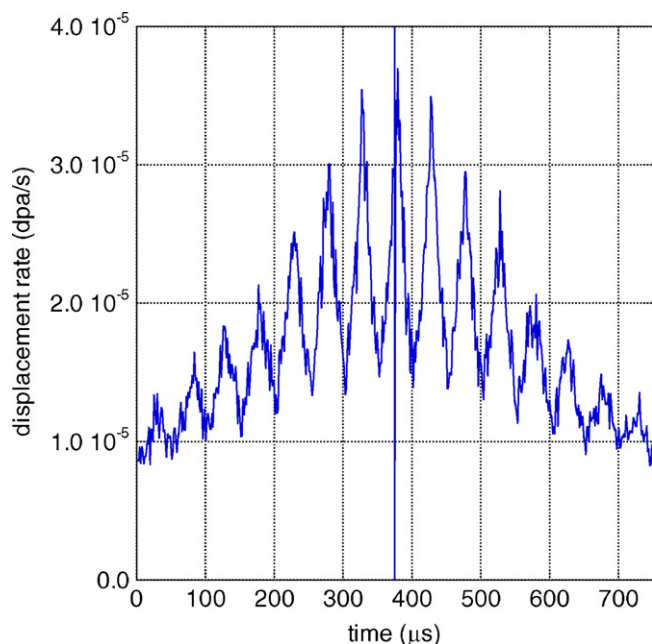


Fig. 8. Displacement rate at the peak flux position for 1-MW beam power.

ation damage region. The simulation assumed 1 MW beam power on target. As mentioned earlier, the displacement rate varies as (beam power)<sup>0.8</sup>. While the nominal F<sup>3</sup> beam power has not yet been fixed, it will probably be in the range of one to several MW.

The atomic displacement tally was placed within a 10-mm-high section of the fuel irradiation region having the highest time-averaged flux, and the beam was directed onto the target closest to this tally volume. The tallied displacement rate for iron is shown in Fig. 8. At 1 MW beam power, the mean displacement rate during a beam macropulse is  $1.68 \times 10^{-5}$  dpa/s, corresponding to a time-averaged rate of  $1.26 \times 10^{-6}$  dpa/s.

Several structures are evident. First, one can see a general upward trend in the dpa rate before 375 μs, and a general downward trend after that, which is due to the vertical slew of the rastered beam. Second, one observes a saw tooth pattern superposed on the trend due to the vertical slew, caused by the horizontal component of the beam raster. The local minima in the saw tooth pattern correspond to the points in time when the beam is at the horizontal position farthest from the fuel irradiation region, while the local maxima occur when the beam is closest to this region.

The displacement rate dependence on the micropulse structure is shown in Fig. 9. The proton micropulse structure is clearly evident in the calculated displacement rate, showing a peak displacement rate of  $3 \times 10^{-4}$  dpa/s, more than 200 times greater than the time-averaged displacement rate. This micropulse simulation is performed at a point in time when the beam is closest to the displacement tally volume. For this case, source neutrons from proton-induced spallation reactions are created as close as 8 mm to the tally volume. It takes a 1-MeV source neutron about 600 ps to traverse this 8 mm distance. Hence it is entirely plausible that the beam micropulse structure would manifest itself in the tallied displacement rate.

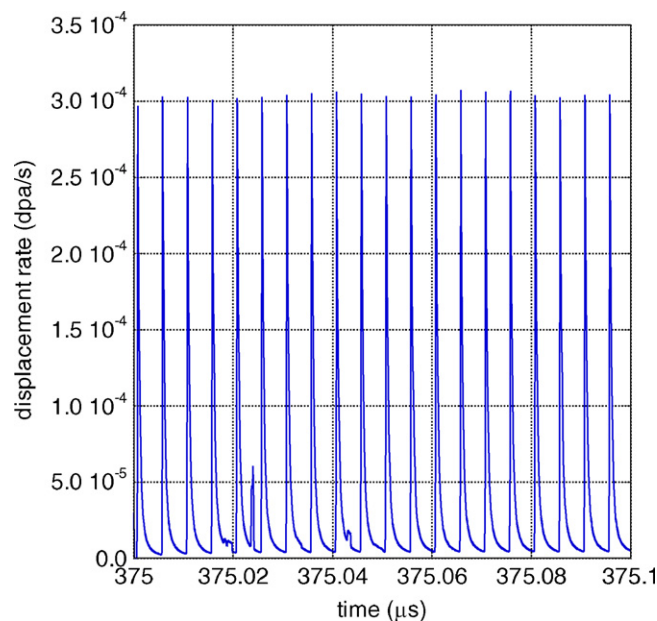


Fig. 9. Displacement rate dependence on beam micropulse structure.

If a significant fraction of iron atoms is involved in damage cascades at any point in time, there is the potential that the cascades may overlap one another, which would likely influence cascade evolution. In a spallation source, the majority of neutrons are born with kinetic energies of a few MeV. Molecular dynamics simulations [9] indicate the volume needed to completely encompass a damage cascade caused by a 2.2-MeV neutron is a cube 30 nm on a side (filled by 2.2 million atoms), and the duration of the cascade is no more than 30 ps. Thus the fraction of atoms involved in a damage cascade during the time of peak displacement rate of  $3 \times 10^{-4}$  dpa/s is  $(3 \times 10^{-4} \text{ displ/atom/s})(2.2 \times 10^6 \text{ atoms/cascade})(30 \text{ ps}) / (216 \text{ displ/cascade}) = 10^{-10}$ . Given this miniscule fraction, the proton beam pulse structure of the F<sup>3</sup> does not produce overlapping cascades.

## Acknowledgments

The author is grateful to Dr. S.P. Simakov of the Karlsruhe Institute of Technology for useful discussions on the method used here for calculating the DEMO HCLL PKA spectrum, and for providing the author with the DEMO HCLL neutron spectrum.

## References

- [1] E. Pitcher, J. Nucl. Mater. 377 (2008) 17.
- [2] E. Pitcher, et al., Proc. 8th Intl. Topical Mtg. on Nuclear Applications and Utilization of Accelerators, Pocatello, USA, July 29–August 2, 2007, p. 82.
- [3] S.P. Simakov, et al., J. Nucl. Mater. 386–388 (2009) 52.
- [4] R.E. MacFarlane, D.W. Muir, The NJOY Nuclear Data Processing System, Version 91, Los Alamos National Laboratory report LA-12740-M, October 1994.
- [5] L.S. Waters (Ed.), MCNPX User's Manual, Los Alamos National Laboratory report LA-CP-02-408, September 2002.
- [6] U. Fischer, et al., J. Nucl. Mater. 280 (2000) 151.
- [7] M.J. Norgett, M.T. Robinson, I.M. Torrens, Nucl. Eng. Des. 33 (1975) 50.
- [8] S.J. Zinkle, M. Victoria, K. Abe, J. Nucl. Mater. 307–311 (2002) 31.
- [9] R. Stoller, J. Nucl. Mater. 276 (2000) 22.